From Vegetation to Vulnerability: Integrating Remote Sensing and AI to Combat Cheatgrass-Induced Wildfire Hazards in California

Srikantnag A. Nagaraja[1,4], Istvan Kereszy[1,2], Chang Zhao[3], and Imre Bartos[1,2,*]

[1]Fire Neural Network, Gainesville, Florida, USA
[2]Department of Physics, University of Florida, Gainesville, Florida, USA
[3]Agronomy Department, UF/IFAS, Gainesville, Florida, USA
[4]Department of Electrical and Computer Engineering, University of Florida, Gainesville, Florida, USA
[*]Corresponding Author: Imre Bartos (email: imrebartos@ufl.edu)

***Abstract*—Wildfire risk is on the rise around the world. In places like California, this risk is further instigated by the invasive species cheatgrass (Bromus tectorum). Cheatgrass is highly flammable and benefits from wildfires, allowing it to replace native plant communities. Through increasing both the intensity and the frequency of wildfires, it endangers not only its natural environment but also human habitats. Here, we present a novel approach to map the distribution and expansion of cheatgrass and predict potential wildfire risk zones. Utilizing the open-source CalFlora dataset, alongside data from the Sentinel–2 satellites, we created a comprehensive spatial analysis framework. We integrated temporal dynamics via Vegetation Index statistical bands that encapsulate annual vegetation information. We employed semi-supervised learning techniques to refine and filter our data labels, thereby ensuring robust model training. We utilized machine learning algorithms Random Forest and XGBoost for model training. Our models exhibited a test accuracy of 91.1% in multiclass classification and achieved a precision rate of $\sim 91\%$ specifically for the Cheatgrass class. Our multiclass classification model demonstrates exceptional discriminative ability and agreement with the actual classifications, with an ROC-AUC Score of 0.99 indicating near-perfect performance in distinguishing between the different classes, and a Cohen's Kappa of 0.89 signifying a strong agreement, accounting for chance. We demonstrate the efficacy of our methodology in identifying regions at high risk of wildfires due to Cheatgrass proliferation, highlighting the potential for broader application across California's diverse landscapes. Our analysis effectively predicts the distribution of Cheatgrass and other vegetation with data available only until June, providing insight before the peak forest fire season, which spans from mid-July to September. This capability delivers actionable intelligence for assessing fuel load and connectivity, thus laying the groundwork for targeted wildfire prevention strategies and enhanced ecological management practices in fire-prone areas.**

***Index Terms*—Land use and Land cover Mapping, Cheatgrass, Invasive Plants, Machine Learning, Semi-supervised Learning, Wildfire Prevention, Time-series Analysis.**

I. Introduction

Wildfires have become a frequent occurrence worldwide, often highlighted for their adverse effects. However, fire also plays a critical role in the health and sustainability of various forest ecosystems. Growing concerns stem from observed trends such as increased fire frequency, extended fire seasons, and the intensified impact of fires being reported globally ([1], [2]). In a long-term study of fire trends through Antarctic ice core analysis[3] identified a 200-year cycle in fire frequency, noting a rise in biomass burning from the 1600s to the 1800s, followed by a decline starting in the 1800s. Today, the heightened wildfire frequency and scale seen in recent decades raise serious concerns about the ecological, socio-economic, and land-resource implications of these fires.

In 2020, California encountered an unprecedented level of wildfire activity, with approximately 1.74 million hectares burned, surpassing the previous record by more than a factor of two. The economic impact of these wildfires was severe, exceeding $19 billion in losses [4]. The resultant smoke significantly contributed to an estimated 0.7 to 2.6 million workdays lost due to PM2.5 exposure, underscoring the considerable health impact [5].

Future projections for areas in California at risk of wildfires indicate a significant transformation in the insurance market by 2055, with a predicted five-percentage-point reduction in the market share of admitted insurers and an 18 percent hike in the rate per $1,000 of coverage [6]. These data highlight the critical need for improved wildfire management strategies to mitigate economic and public health impacts in the future.

The dynamics of wildfires are shaped by numerous complex factors. These include the decline in summer precipitation across the Western United States [7], terrain variations [8], and the availability and connectivity of combustible materials. Additionally, the source of ignition plays a crucial role in the spread of wildfires.

Lightning stands as the foremost natural cause of ignition for wildfires in the U.S., responsible for 15% of these events and 60% of the total area burned [9]. Fires started by lightning typically occur in remote and hard-to-access locations, which complicates their detection and suppression efforts [10]. Notably, in 78% of these incidents, the first house destruction occurred one day post-ignition. Moreover, wildfires initiated by lightning tend to cover larger areas compared to those caused by human activities [11]. The age of fuels also influences ignition patterns, with older fuels (over 25 years) more prone to lightning strikes and younger fuels (less than 10 years) more susceptible to arson [12]. Consequently, understanding and mapping fuel connectivity is pivotal in managing the spread of lightning-triggered wildfires.

Cheatgrass, an invasive non-native annual grass, significantly impacts the fire regimes across the Intermountain West, particularly in the Great Basin. It negatively affects the richness and abundance of small mammals [13], [14] and degrades habitat for the Greater Sage-Grouse [15], [16], a species vital for regional ecological management. By increasing the connectivity and availability of fine fuels, Cheatgrass leads to more frequent fires compared to those in native ecosystems [17], [18]. Post-fire scenarios often

result in Cheatgrass dominance, making recovery for native shrubs and grasses particularly challenging, especially in hotter and drier regions [19]. The severe ecological consequences of Cheatgrass invasion highlight the importance of accurate regional modeling of its spread and density to develop effective management strategies.

The distinct phenological traits of Cheatgrass, compared to native vegetation, enhance its detectability via satellite imagery. The earlier phenology of invasive plants, such as Cheatgrass, often gives them a competitive advantage over native species [20]. These phenological differences facilitate the satellite detection of invasive species [21]. For instance, Cheatgrass exhibits early spring productivity before native shrubs and grasses, leading to a shift in the timing of peak greenness that is detectable through satellite time series [22]. Leveraging Sentinel–2 satellite data, we applied this phenological analysis by utilizing time series satellite data and successfully achieved the classification of Cheatgrass.

Creation of digital Land use and land cover(LULC) datasets using various remote sensing techniques can be an effective approach, to effectively monitor and assess these changes [23]. Many attempts have been made to map the LULC since very long using various supervised and unsupervised algorithms ([24], [25], [26]). Previous work on Cheatgrass distribution mapping utilized fuelscape datasets at a 270-meter resolution, covering the sagebrush biome of the western United States [27]. Pastick et al. [28] established a foundational methodology for mapping invasive annual grasses using harmonized Landsat and Sentinel-2 (HLS) data, focusing on NDVI time series and phenological metrics. While effective, their approach mainly utilizes NDVI, which may not fully leverage the additional insights provided by other spectral bands. Furthermore, their method primarily incorporates a limited timeframe of data, which might affect the ability to capture broader seasonal variations. Additionally, the mapping approach is designed for general exotic annual grasses, which may not achieve the same specificity needed for Cheatgrass detection. The San Bernardino County Fire Department (SBC) [29] is responsible for managing wildland fires in the United States largest county. SBC has successfully implemented a GIS-based Community Wildfire Protection Plan (CWPP) that integrates out cheatgrass data to effectively target this invasive plant during prescribed burns and other fuel mitigation actions.

This paper utilizes Sentinel-2 imagery at a finer 10-meter resolution than previous work, and integrates both reproductive season data (May and June) and year-long(July-June) phenological observations through vegetation index distribution bands. By adopting the user-generated Calflora [30] dataset, which is more commonly available and offers finer temporal resolution, we focus specifically on Cheatgrass, enabling precise and timely mapping before the forest fire season in July. This approach ensures the availability of up-to-date maps and the integration of real-time datasets, significantly enhancing the effectiveness of wildfire management and invasive species monitoring.

The objectives of this research are centered around the detailed study and management of vegetation in wildfire-prone areas, with particular focus on Cheatgrass. These objectives are the following:

- Utilize satellite remote sensing and the open-source Calflora Dataset for land use and land cover mapping, with a focus on mapping Cheatgrass distribution.
- Determine temporal variation in the spread of Cheatgrass to understand risks and causes.
- Demonstrate the creation of accurate, annual pre-fire-season vegetation maps that can aid planning and management.

These objectives aim to provide a comprehensive approach to managing vegetation in fire-prone regions, with a particular emphasis on understanding and controlling Cheatgrass to reduce wildfire risk and its ecological impact.

II. Data and Methodology

A. Sentinel–2 Data Acquisition and Preprocessing

The Copernicus Sentinel-2 mission consists of two polar-orbiting satellites positioned in the same sun-synchronous orbit, with a phase difference of 180°. This configuration aims to monitor changes in land surface conditions efficiently. Equipped with a multispectral imager (MSI) that has 13 spectral bands, Sentinel-2 provides moderate resolution imagery with a swath width of 290 km. This wide swath and the high revisit time enable global coverage every five days, supporting the continuous monitoring of the Earth's surface. The primary objectives of the Sentinel-2 satellites include providing data for risk management, land use and land cover mapping, change detection, natural hazards, and water management. These capabilities are crucial for a wide range of applications in environmental monitoring and management [31]. We acquired the Sentinel-2 images using Google Earth Engine [32].

We applied a bilinear interpolation technique to enhance the resolution of specific spectral bands at 20 meters to a uniform 10 meters in order to maintain consistent resolution across all bands. Bilinear interpolation was chosen because the bands represented continuous imagery, rather than segmentation[33]. This refinement was applied to those bands originally at 20-meter resolution, resulting in a consistent 10-meter resolution across the selected bands. Here, we used a total of ten spectral bands ranging from the visible to the shortwave infrared wavelengths (Table I)([34]). As an initial step, Sentinel–2 Surface Reflectance (SR) images with less than 20% cloud coverage were systematically selected for the months of May and June 2022.

In our time series analysis, addressing the significance of cloud interference is essential. To reduce this issue, we first utilized the Cloud Probability Band from Sentinel-2 Level-2A products [35], using its inverse as a key factor in creating mosaics of temporal imagery, effectively minimizing noise. Next, we filtered out snow and cloud pixels by applying masks [35], [36]. These combined techniques greatly reduced noise, providing a strong method for time series analysis in our study. During the masking process, the results were visually inspected, and all parameters were refined through multiple iterations to ensure optimal outcomes across all months.

B. Dataset

The Calflora dataset [30] was utilized to examine the occurrence of Cheatgrass (*Bromus tectorum*) across California (Figure 2). This comprehensive database provides critical georeferenced data on wild plant species within the state, supporting various ecological studies. The dataset includes detailed species-specific information and insights into plant distributions, which are instrumental in

TABLE I: Sentinel–2A Bands Used

Band	Resolution	Central Wavelength	Description
B2	10m	490 nm	Blue
B3	10m	560 nm	Green
B4	10m	665 nm	Red
B5	20m	705 nm	VNIR
B6	20m	740 nm	VNIR
B7	20m	783 nm	VNIR
B8	10m	842 nm	VNIR
B8a	20m	865 nm	VNIR
B11	20m	1610 nm	SWIR
B12	20m	2190 nm	SWIR

Note: VNIR refers to Visible and Near Infrared; SWIR refers to Shortwave Infrared.

understanding the spread and habitat preferences of plant species. Specifically, this resource is essential for tracking the temporal and spatial dynamics of Cheatgrass, an invasive species with significant ecological impacts. But since this dataset had many inaccuracies as shown in Figure 1

Fig. 1: Some inaccuracies in Caflora [30] dataset with High-resolution Imagery Background[37]

C. Labeling and Refining

Our research commenced with systematically gathering Cheatgrass sample locations from the CalFlora dataset [30] for Los Angeles County, spanning the period from January 1, 2016, to January 10, 2024. Los Angeles County was selected due to its ecological diversity, encompassing coastal areas, mountain ranges, valleys, forests, islands, lakes, rivers, and deserts [38], making it representative of broader Californian landscapes. To categorize

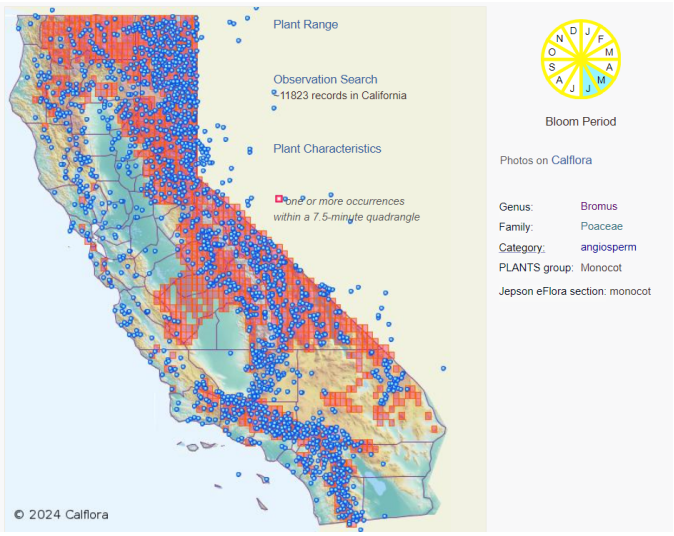

Fig. 2: A screenshot of Cheatgrass Data from Calflora Website [30]

regions by land cover type—such as water, grass, shrubland, trees, and bareland—the Dynamic World V1 Land Cover map was employed [39]. Each sample was meticulously verified using Sentinel-2 imagery from April and June 2022, focusing on distinguishing color contrasts in the RGB bands within Los Angeles County. This process was further cross-checked with high-resolution Imagery base-map in ArcGIS PRO [37]. Given that Cheatgrass often grows in patches around 300 m² [40], the 10-meter resolution of Sentinel-2 proved valuable for identifying pure pixels. Points that appeared to be mixed on high-resolution images were relocated to the nearest pixel that accurately represented the targeted vegetation type. This detailed approach produced a dataset of 650 samples across six distinct land cover types: Grassland, Shrubland, Bareland, Water, Cheatgrass, and Trees (Table II).

TABLE II: Initial 650 samples

Category	Sample Size
Trees	205
Grassland	38
Shrubland	233
Bare Soil	34
Water	30
Cheatgrass	110
Total	650

In the data preparation phase, we addressed the inherent inaccuracies in some user-reported entries within the Calflora dataset(Figure 1), specifically focusing on Cheatgrass samples. For each Cheatgrass point across California from the Calflora dataset, we established a 200-meter buffer zone and generated four random peripheral points, resulting in a total of five distinct sampling points for each original location.

These points were then used to extract spectral values from Sentinel-2 imagery captured in April and June. The extracted data was input into a Binary Multilayer Perceptron (MLP) Classifier [41] (Figure 3), which was trained using 80% of the dataset, while the remaining 20% was reserved for validation (Table II).

We tested various probability thresholds between 0.4 and 0.7, evaluating the relationship between the number of input points labeled as Cheatgrass and the classifier's output labels.Setting the probability threshold to 0.5 yielded an optimal balance, as it selected one confirmed point plus four additional points randomly within a defined buffer around each positive instance. This threshold effectively reduced noise, eliminating 4 out of every 5 generated samples around each point. Finally, the retained samples were randomly validated visually to ensure classification accuracy. More detailed results of this MLP classifier are provided in Appendix A. Figure 4 illustrates how the inaccuracies of the Calflora dataset are corrected by this MLP Classifier.

```
Model: "sequential_2"
_________________________________________________________________
 Layer (type)                Output Shape              Param #
=================================================================
 dense_8 (Dense)             (None, 256)               5376

 dropout_6 (Dropout)         (None, 256)               0

 dense_9 (Dense)             (None, 128)               32896

 dropout_7 (Dropout)         (None, 128)               0

 dense_10 (Dense)            (None, 64)                8256

 dropout_8 (Dropout)         (None, 64)                0

 dense_11 (Dense)            (None, 1)                 65

=================================================================
Total params: 46,593
Trainable params: 46,593
Non-trainable params: 0
_________________________________________________________________

Optimizer: Adam
Loss: Binary Crossentropy
Metrics: Accuracy
```

Fig. 3: Binary Multilayer Perceptron (MLP) Architecture

This binary classification approach was replicated across all classes, leading to a refined set of labeled samples. Finally, we amalgamated the refined dataset of 650 samples to train a comprehensive multiclass classifier. This classifier aimed to effectively distinguish between the defined classes, leveraging the refined and accurately labeled dataset to enhance the predictive accuracy and reliability of the model. Finally we had 8855 samples across 6 classes as shown in Table III.

TABLE III: Final Sample Design

Category	Sample Size
Trees	1997
Grassland	1055
Shrubland	2268
Bare Soil	1498
Water	298
Cheatgrass	1739
Total	8855

This kind of label refining method would help us to integrate datasets like iNaturalist in the future[42].

D. Time Series Spectral Bands

Given the annual lifecycle of Cheatgrass, effectively predicting its proliferation requires a detailed understanding of its temporal

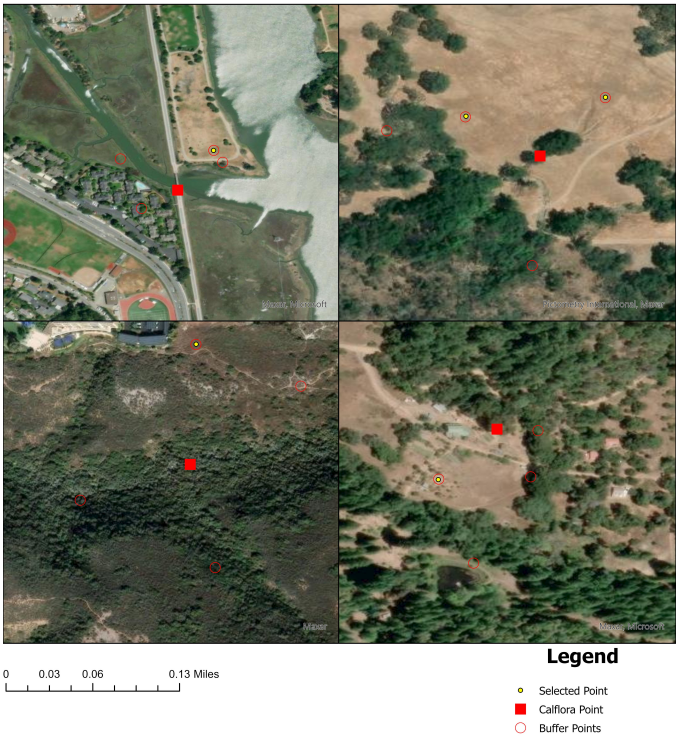

Fig. 4: Label Refining using MLP with High-resolution Imagery Background[37].

variability. The bloom period of Cheatgrass, typically spanning May to June, serves as a key temporal indicator that differentiates it from other vegetation. To leverage this distinct seasonal behavior, we introduced an innovative set of features derived from the temporal dynamics observed in spectral data. Specifically, we utilized data from May 2022 and June 2022 to inform our analysis.

To incorporate indirect time series information for each pixel over a year, we employed a novel approach by generating statistical bands. These bands encapsulate the skewness, kurtosis, mean, and standard deviation of three key vegetation indices: NDVI [43], GNDVI [44], and MSAVI2 [45], covering the period from July of the previous year to June of the prediction year. This integration added twelve additional layers to our model, significantly enriching the dataset with temporal insights and enhancing the model's accuracy in distinguishing Cheatgrass from other vegetation types. Prior to calculating the skewness, kurtosis, mean, and standard deviation bands, monthly mosaicked Sentinel-2 images [35] were processed to derive NDVI, GNDVI, and MSAVI2, which were then used to compute the statistical bands.

Figure 5 illustrates how the NDVI distribution varies across different land cover classes over the months and highlights how metrics such as Mean, Standard Deviation, Kurtosis, and Skewness of monthly vegetation index can aid in distinguishing between these classes.

This methodology underscores the importance of integrating time-sensitive spectral differences and statistical analyses to improve the predictive modeling of Cheatgrass, ensuring robustness across varying temporal scales.

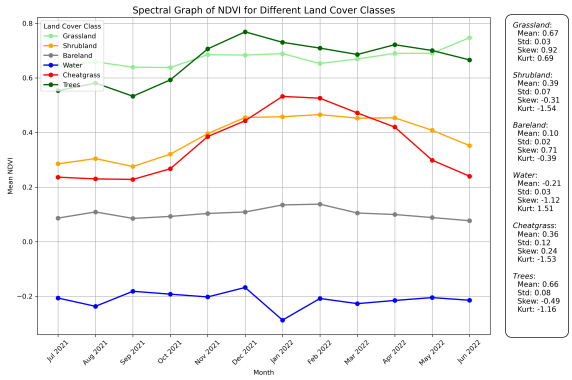

Fig. 5: NDVI variation across different classes from July 2021 to June 2022.

E. Classification Algorithm

We applied two powerful ensemble machine learning algorithms, XGBoost and Random Forest (RF), to identify Cheatgrass. XGBoost, known for its efficiency in classification tasks [46], leverages an ensemble of decision trees to boost classification accuracy. Its high predictive power is due to its effective loss function and the optimization of weak learners, leading to superior model performance [46], [47], [48]. The algorithm's iterative and additive training process, combined with a stringent regularization framework, ensures robustness against overfitting [49], [13]. Detailed mathematical insights into this algorithm are thoroughly documented in Chen's works [46].

The Random Forest (RF) algorithm [50] employs bootstrapping to generate numerous decision trees from different data samples. Each decision tree utilizes the Classification and Regression Trees (CART) algorithm to split nodes by minimizing Gini Impurity, which quantifies the likelihood of a misclassification if a new random variable were assigned a random label based on the training sample distribution. The overall classification is performed through bootstrap aggregation. This method was selected due to its proven high accuracy in recent studies, particularly in land cover classification tasks [51], [47], [52]. Comprehensive details of the RF algorithm can be found in specialized literature [50], [53].

F. Example use case

Our study examines two significant wildfire cases: the El Dorado Fire of 2020 and the Corral Fire of 2024, highlighting the role of cheatgrass invasion in post-fire fuel accumulation and its contribution to fire spread. The El Dorado Fire, which burned approximately 22,744 acres (9,204 ha; 35.538 sq mi; 92.04 km²) across San Bernardino and Riverside counties, was ignited on September 5, 2020, by a pyrotechnic device in El Dorado Ranch Park and quickly expanded into the San Gorgonio Wilderness Area within the San Bernardino National Forest. The fire burned for 71 days, destroying 20 structures and resulting in a firefighter fatality [54].

To analyze vegetation dynamics pre- and post-fire, we focused on a 100-mile by 100-mile region encompassing the El Dorado fire perimeter (Table X), allowing us to compare vegetation changes within the burned area to surrounding areas not impacted by the fire. The land use and land cover (LULC) data for 2020 were collected up to June, just before the fire's occurrence in September. Since the West Coast's proximity introduced marine areas into this 100-mile radius—irrelevant to our study—we adjusted the centroid 20 miles northeast to focus exclusively on terrestrial changes (Figure 13).

In contrast, the Corral Fire of 2024 in San Joaquin County illustrates the rapid spread typical of grass-fueled wildfires. Detected at 4:44 pm on June 1, it reached over 9,000 acres in just five hours, achieving this scale by 9:46 pm, and ultimately consumed 14,168 acres [55]. According to the National Interagency Fire Center's Incident Management Situation Report, suppression efforts for the Corral Fire cost approximately $3.4 million [56]. This swift expansion highlights the need for advanced predictive models and monitoring systems to effectively manage and mitigate such rapidly advancing fires.

Additionally, Appendix B demonstrates our model's predictive capabilities in classifying shrubland-dominated areas in the Mojave Desert, illustrating the LULC model's robustness in capturing diverse landscapes and terrain types. This example underscores the model's potential in broader applications across various ecosystems and fire-prone environments.

III. Results and Discussion

A. Classification Accuracy

We split the dataset(Table III) 80:20, training our models with 80% of the data and using the remaining 20% for testing.

Additionally, we examined the variance in band intensities between June 2022 and April 2022, as well as 12 time series statistical bands, applying a scaling factor derived from the 1st percentile minimum and maximum values within Los Angeles County.

We subsequently trained models using the Random Forest and XGBoost algorithms, which were further refined through rigorous hyperparameter tuning via a 10-fold grid search(Table IV).

Model	Parameter	Values
Random Forest	min_samples_split	{2, 3, 5, 6, 7, 8, 10}
Random Forest	n_estimators	{250, 500, 1000, 2000, 3000}
XGBoost	n_estimators	{200, 500, 1000, 3000, 5000}
XGBoost	learning_rate	{0.1, 0.05, 0.01, 0.005, 0.001}

TABLE IV: Parameter Grid for 10-Fold Grid Search on Random Forest and XGBoost Models

Despite achieving an initial model accuracy of 95%, we encountered challenges in generalizing across different years and counties, partly due to the specific scaling applied using the 1st percentile minimum and maximum values from Los Angeles County. Additionally, residual snow in April led to incorrect predictions for the water class. To address these issues, we refined our dataset to include only observations from May and June 2022, corresponding to the Cheatgrass bloom period. We also incorporated twelve unaltered statistical bands from three vegetation indices to enhance the model's robustness. Data was extracted to labels from bands shown in table V. Although this adjustment slightly reduced the overall model accuracy to 91.1%, it significantly improved the model's reliability and performance across both temporal and spatial dimensions.

TABLE V: Bands used to extract values for labels.

Data	Date	No. of Bands
June Sentinel-2	06/01/2022 to 06/30/2022	10
May Sentinel-2	05/01/2022 to 05/31/2022	10
NDVI Distribution Bands	07/01/2021 to 06/30/2022	4
GNDVI Distribution Bands	07/01/2021 to 06/30/2022	4
MSAVI-2 Distribution Bands	07/01/2021 to 06/30/2022	4

Note: Distribution bands are Mean, Standard Deviation, Skewness, Kurtosis.

TABLE VI: Classification Accuracy and Confusion Matrix for Random Forest.

True/Predicted	GS	SH	BR	WT	CG	TR
GS	189	0	0	0	**1**	21
SH	2	397	1	0	**34**	17
BR	0	1	298	0	**0**	1
WT	0	0	0	60	**0**	0
CG	**0**	**45**	**2**	**0**	**294**	**6**
TR	14	16	0	1	**1**	367
Column Total	211	450	300	60	**347**	399
Precision (UA)	0.92	0.86	0.99	0.98	**0.89**	0.89
Recall (PA)	0.90	0.88	0.99	1.00	**0.85**	0.92
Overall Accuracy	**0.908**					
Kappa	**0.885**					

Note: GS - Grassland, SH - Shrubland, BR - Bareland, WT - Water, CG - Cheatgrass, TR - Trees, UA - User accuracy, PA - Producer accuracy.

TABLE VII: Classification Accuracy and Confusion Matrix for XGBoost.

True/Predicted	GS	SH	BR	WT	CG	TR
GS	187	0	0	0	**1**	23
SH	1	403	0	0	**29**	17
BR	0	1	297	0	**1**	1
WT	0	0	0	59	**0**	1
CG	**1**	**43**	**1**	**0**	**299**	**3**
TR	15	18	0	1	**0**	365
Column Total	211	450	300	60	**347**	399
Precision (UA)	0.92	0.87	1.00	0.98	**0.91**	0.89
Recall (PA)	0.89	0.90	0.99	0.98	**0.86**	0.91
Overall Accuracy	**0.911**					
Kappa	**0.889**					

Note: GS - Grassland, SH - Shrubland, BR - Bareland, WT - Water, CG - Cheatgrass, TR - Trees, UA - User accuracy, PA - Producer accuracy.

The ROC curves shown in Figures 6 and 7 provide a detailed evaluation of classifier performance for each class. The Random Forest model's ROC curves (Figure 6) demonstrate high AUC values for most classes, with the Grassland, Bareland, and Water classes achieving perfect scores (AUC = 1.00). The Shrubland and Cheatgrass classes show slightly lower AUC values of 0.98, indicating some misclassification errors. Similarly, the XGBoost model (Figure 7) exhibits high AUC values across all classes, with Grassland, Bareland, and Water also achieving perfect AUC scores. The Cheatgrass and Trees classes have slightly lower AUC values of 0.98 and 0.99, respectively, indicating robust performance with minor classification errors. These high AUC values across both

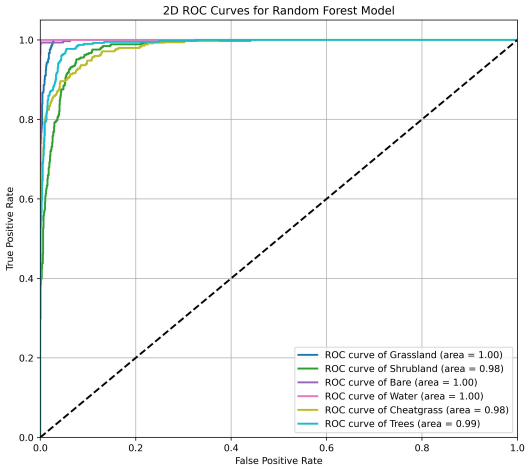

Fig. 6: Random Forest Model ROC Graphs.

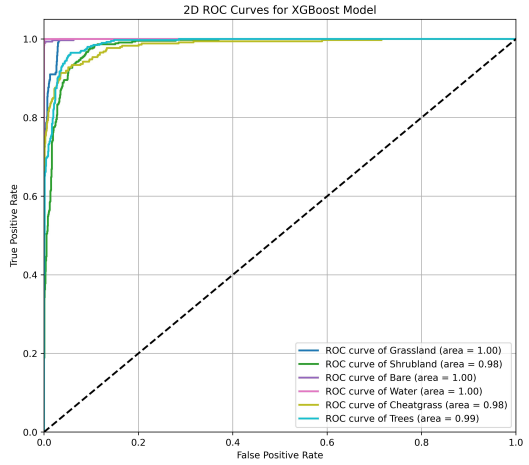

Fig. 7: XGBoost Model ROC Graphs.

models affirm the robustness of our approach in distinguishing between different land cover classes.

The confusion matrix (Table VI and Table VII) indicates challenges in accurately classifying Shrubland within our dataset. However, the high precision in identifying Cheatgrass confirms the effectiveness of our modeling approach. Currently, our analyses rely on static 2022 data. To enhance the robustness of model performance and increase temporal diversity, raising public awareness about Cheatgrass is crucial. Encouraging the collection of Cheatgrass location data, including precise latitude and longitude coordinates, could help in obtaining high-quality data. Additionally, developing an application for the public to report Cheatgrass locations could provide a large quantity of data. This data can be filtered using a semi-supervised MLP model designed for extracting extra labels, thereby improving our dataset and enabling the development of more sophisticated models. This approach would enhance our analytical capabilities and improve predictive accuracy across diverse

TABLE VIII: Bands used to extract LULC Map Figure 8 and Figure 9

Data	Date	No. of Bands
June Sentinel-2	06/01/2024 to 06/30/2024	10
May Sentinel-2	05/01/2024 to 05/31/2024	10
NDVI Distribution Bands	07/01/2023 to 06/30/2024	4
GNDVI Distribution Bands	07/01/2023 to 06/30/2024	4
MSAVI-2 Distribution Bands	07/01/2023 to 06/30/2024	4

Note: Distribution bands are Mean, Standard Deviation, Skewness, Kurtosis.

ecological scenarios.

B. LULC Map

Figure 8 shows the Land Use Land Cover (LULC) map for California State 2024, generated using the trained XGBoost model with 32 bands (Table VIII). Figure 9 represents the probability map of the class Cheatgrass derived using the trained XGBoost model with 32 bands (Table VIII). This LULC and Cheatgrass Probability map enables the analysis of fuel connectivity, revealing areas with high Cheatgrass density. Additionally, regions where forests are surrounded by Cheatgrass pose a significant risk of large forest fires due to potential ignition sources and fuel connectivity. The analysis excluded built-up and cropland classes because of their heterogeneous landscapes and varying spectral characteristics, especially croplands whose spectral signatures change with the agricultural season. For Figure 8, for built-up areas, the GHSL: Global Settlement Characteristics (10 m) 2018 (P2023A)[57] dataset was used, which is at 10 m resolution. For cropland, the USDA NASS Cropland Data Layers[58], were used from the period between '2016-01-01' and '2017-12-31'. While mosaicking cropland and built-up areas, Cheatgrass pixels were given priority.

Figure 8 also illustrate a strong correlation between vegetation cover and wildfire incidence patterns, significantly influenced by the classes "Trees" and "Cheatgrass". These maps can be utilized to calculate historical fuel loads and assess fuel connectivity at both macro and community levels. The subsequent subsections provide examples demonstrating their potential for both preventive strategies and post-fire behavior analysis.

C. Example use case: El Dorado Fire 2020 Analysis

The El Dorado Fire was a wildfire that burned 22,744 acres (9,204 ha; 35.538 sq mi; 92.04 km2) in San Bernardino and Riverside counties of California from September to November 2020. It was ignited on September 5 by a pyrotechnic device in the El Dorado Ranch Park; it quickly spread to the San Gorgonio Wilderness Area of the San Bernardino National Forest. Burning over a 71-day period, the fire destroyed 20 structures and resulted in one firefighter fatality [54].

We focused on the 2020 El Dorado wildfire to assess vegetation dynamics pre and post-wildfire within a designated 100 by 100 mile (Table X) area surrounding the El Dorado fire boundary. It is important to note that the land use and land cover (LULC) map (Figure 12) for 2020 was compiled using data collected only up until June 2020, two months prior to the actual occurrence of the El Dorado fire in September 2020. Given the proximity of the West Coast—within a 100-mile radius from the fire zone—which

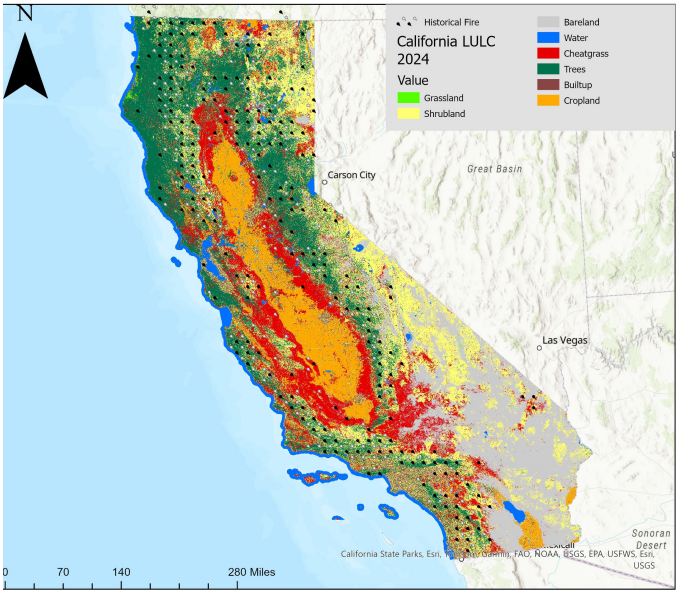

Fig. 8: LULC Map of California 2024.

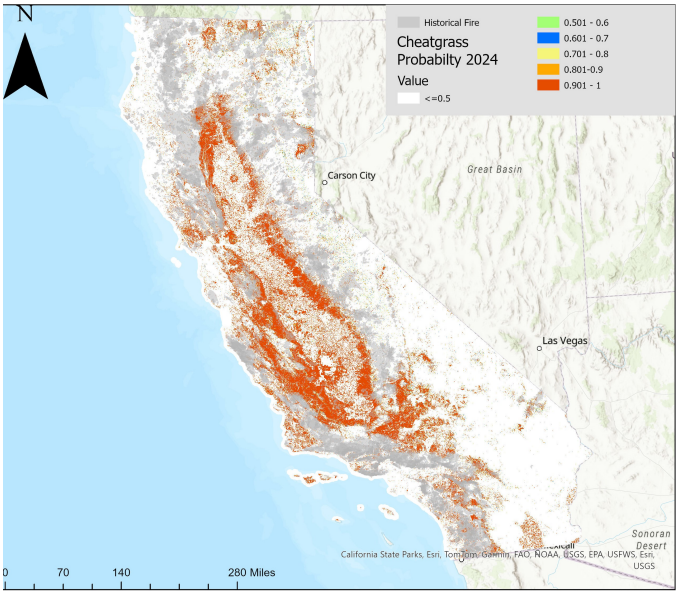

Fig. 9: Cheatgrass Probability Map of California 2024.

included parts of the ocean, and considering that marine areas are not relevant to our study, we adjusted the centroid of the mapped area 20 miles northeast to better focus on the terrestrial environment (Figure 13).

In 2020, recognized as one of the most severe wildfire seasons, the combined presence of trees and Cheatgrass, which constitute critical wildfire fuels, was observed to be 22.52% within the 100 by 100 mile (Table X and Figure 11) area and alarmingly higher at 66.05% within the El Dorado fire region itself (Table IX and Figure 10) . Post-fire assessments indicated a predictable increase in Cheatgrass across the burnt landscape, while fuel loads began to normalize within the fire-affected region from 2020 to 2023 (Table IX and Figure 12). This analysis not only provides insight into the immediate effects of wildfires on local vegetation dynamics but also

TABLE IX: Land Cover Percentages around El Dorado Fire 2020

2020

Land Cover Type	Percentage
Grassland	1.91%
Shrubland	31.00%
Bareland	0.92%
Water/Snow	0.12%
Cheatgrass	13.55%
Trees	52.50%

2021

Land Cover Type	Percentage
Grassland	0.09%
Shrubland	38.97%
Bareland	5.46%
Water/Snow	6.01%
Cheatgrass	48.06%
Trees	1.40%

2022

Land Cover Type	Percentage
Grassland	0.17%
Shrubland	46.66%
Bareland	5.49%
Water/Snow	0.45%
Cheatgrass	45.07%
Trees	2.15%

2023

Land Cover Type	Percentage
Grassland	0.30%
Shrubland	64.97%
Bareland	5.26%
Water/Snow	0.08%
Cheatgrass	22.99%
Trees	6.40%

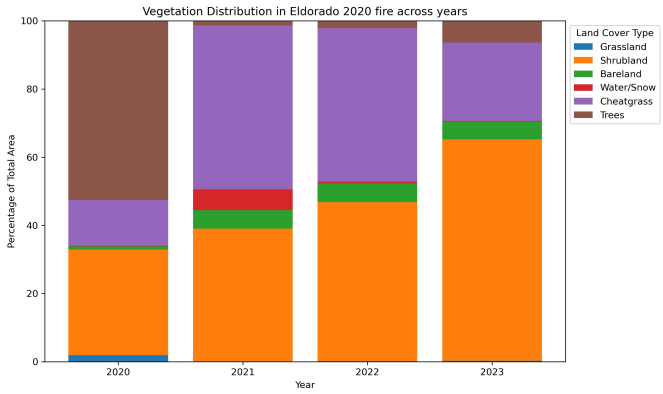

Fig. 10: Vegetation Distribution inside El Dorado Fire 2020 boundary across years.

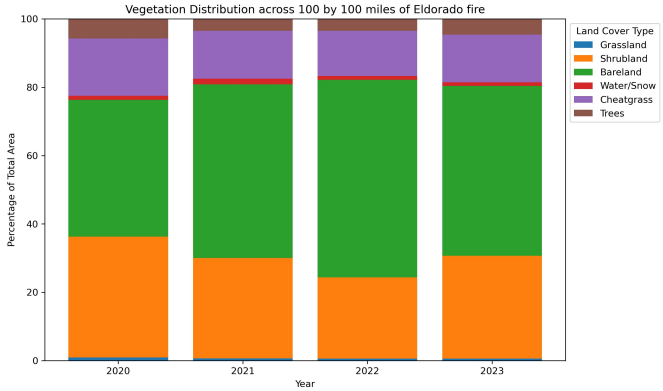

Fig. 11: Vegetation Distribution around 100 by 100 mile of El Dorado Fire 2020 across years.

opens avenues for further research into historical wildfire patterns and the complex interactions between wildfire occurrences and the availability and connectivity of combustible materials.

TABLE X: Land Cover Percentages around 100 by 100 miles

2020

Land Cover Type	Percentage
Grassland	0.95%
Shrubland	35.36%
Bareland	39.98%
Water/Snow	1.20%
Cheatgrass	16.79%
Trees	5.73%

2021

Land Cover Type	Percentage
Grassland	0.69%
Shrubland	29.34%
Bareland	50.81%
Water/Snow	1.64%
Cheatgrass	14.01%
Trees	3.51%

2022

Land Cover Type	Percentage
Grassland	0.60%
Shrubland	23.78%
Bareland	57.78%
Water/Snow	1.10%
Cheatgrass	13.24%
Trees	3.50%

2023

Land Cover Type	Percentage
Grassland	0.61%
Shrubland	30.05%
Bareland	49.74%
Water/Snow	1.06%
Cheatgrass	13.96%
Trees	4.58%

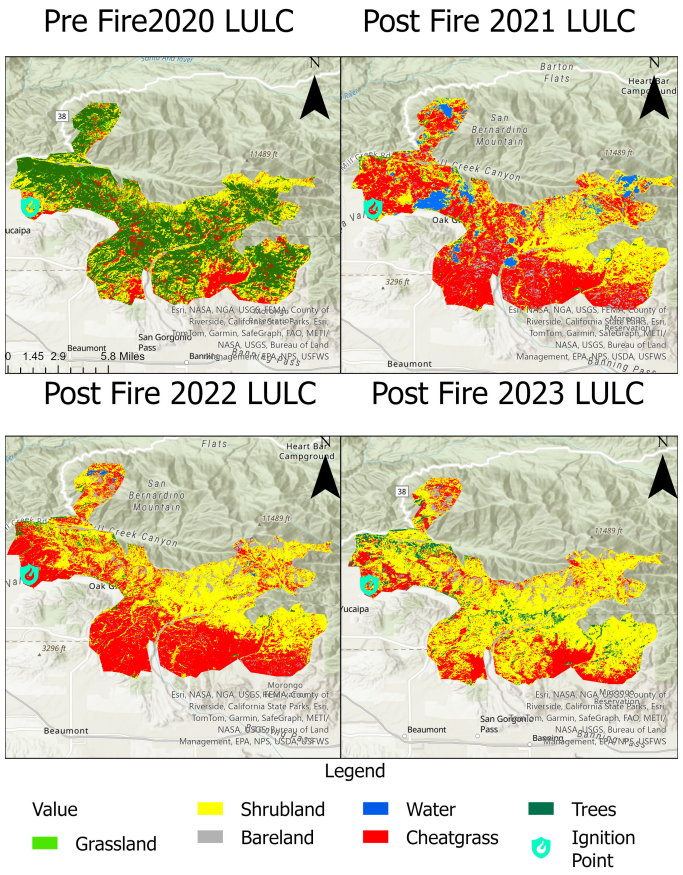

Fig. 12: Pre and Post Land Cover Change in El Dorado Fire 2020

D. Example use case 2: Corral Fire 2024

Our model predicted a significant presence of Cheatgrass from 2020 to 2023 (Figure 14), indicating substantial fuel loads across these years. This finding highlights the importance of incorporating both current and historical Land Use Land Cover (LULC) maps that include Cheatgrass for pre-wildfire preparation tasks. Such maps are crucial for understanding and mitigating wildfire risks.

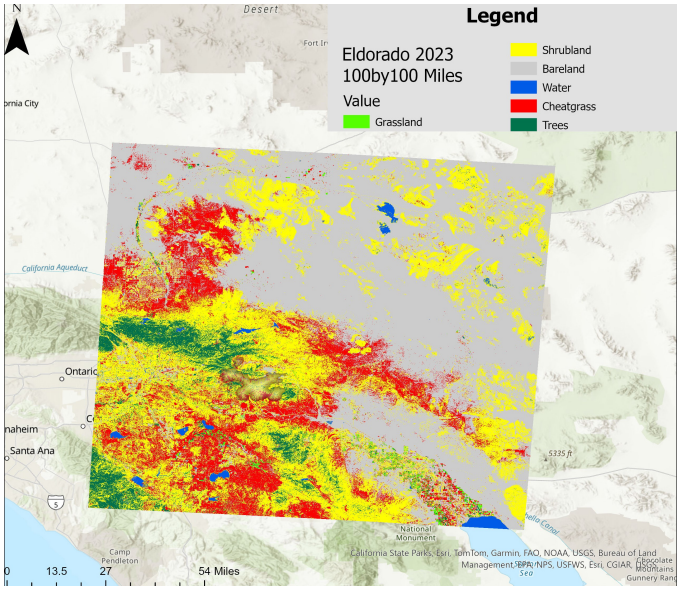

Fig. 13: LULC Map of 2023 around 100 by 100 mile of El Dorado Fire 2020.

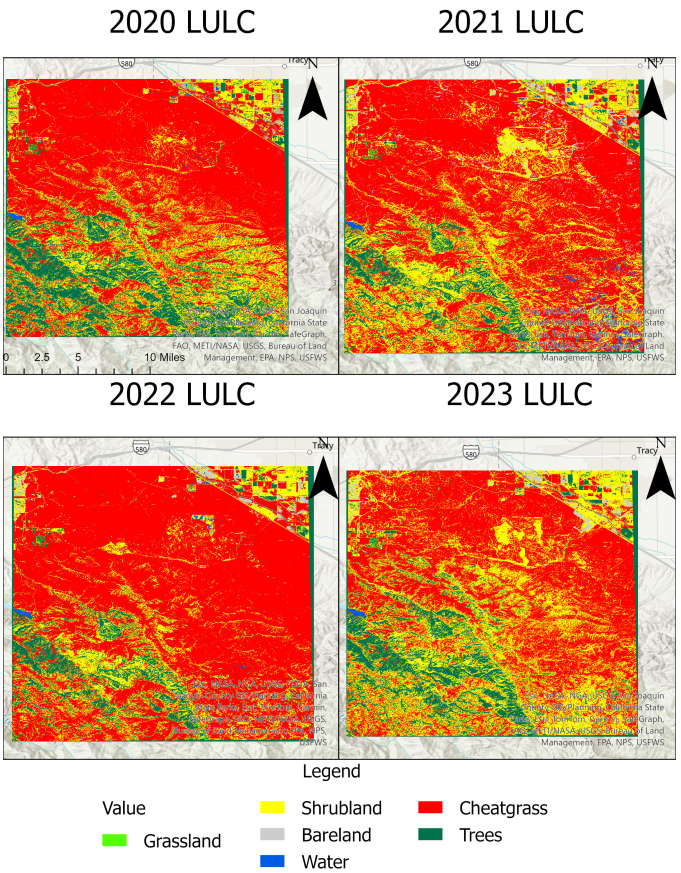

Fig. 14: LULC around Corral Fire 2024

IV. Conclusion

This study presents a robust framework for the early detection and spatial mapping of Cheatgrass (Bromus tectorum), a highly flammable invasive species that amplifies the frequency and intensity of wildfires in California. By integrating the CalFlora dataset with Sentinel–2 Surface Reflectance data and enhancing it with semi-supervised learning, our model achieved an overall accuracy of 91.1% and precision of $\sim 91\%$ in identifying Cheatgrass.

A critical advancement of our research is the model's capacity to perform vegetation mapping and risk assessment before the peak of the wildfire season. By effectively incorporating annual vegetation dynamics through innovative Vegetation Index statistical bands, the model provides actionable insights as early as July, well ahead of the typical wildfire peak from mid-July to September. This timely mapping is pivotal for fire management authorities, allowing for proactive measures such as the strategic deployment of firefighting resources, the implementation of fire breaks, and community alerts in areas predicted to be at high risk.

With Cheatgrass known impact on wildfire dynamics, our framework can serve as a vital tool in forecasting and mitigating the potential spread and severity of fires. The adaptability of our approach also suggests that it could be refined further with incoming data from future growth cycles, improving the model's accuracy and applicability in real-time wildfire prediction.

In conclusion, the methodologies developed through this research not only underscore the feasibility of using machine learning techniques to tackle ecological challenges but also highlight the potential of predictive modeling in wildfire management. As Cheatgrass continues to influence fire regimes, the ongoing adaptation and enhancement of our model will be crucial. Future research should focus on expanding the geographic scope and integrating more dynamic environmental data to enhance predictive accuracy, thereby supporting broader wildfire management strategies and ecological conservation efforts. This proactive approach could significantly contribute to mitigating the ecological and economic impacts of wildfires in California and similar regions globally, aligning with the urgent need for innovative solutions in the face of climate change.

Acknowledgment

The authors acknowledge the support of the University of Florida and Fire Neural Network.

Data Availability

The data is available on request to authors.

Appendix

A. Binary Multilayer Perceptron (MLP) Classifier

Data for Cheatgrass (Bromus tectorum) were extracted from the Calflora database [30], covering the period from January 1, 2016, to January 10, 2023, resulting in 1,720 initial points. To expand the dataset, we generated four random buffer points within a 200-meter radius around each original point. The combined dataset was then input into a binary MLP classifier. We evaluated probability thresholds ranging from 0.4 to 0.7, with a threshold of 0.5 yielding 1,629 positive samples, closely aligning with the initial Calflora points(Table XII. These selected points underwent visual validation using high-resolution imagery in ArcGIS Pro [37]. Table XI provides the classification report for the binary MLP model. Figure 15 represents loss and accuracy curves of train and test. For

additional classes (trees, shrubland, bareland, water, and grassland), stratified random samples were drawn from a dynamic LULC map of Los Angeles County and refined through a similar binary MLP classifier.

TABLE XI: Classification Report for Cheatgrass Detection

Class	Precision	Recall	F1-Score	Support
Non-Cheatgrass	1.00	0.99	1.00	108
Cheatgrass	0.96	1.00	0.98	22
Accuracy				0.99
Macro Average	0.98	1.00	0.99	130
Weighted Avg	0.99	0.99	0.99	130

TABLE XII: Cheatgrass Sample Selection and MLP Processing Details

Description	Count
Cheatgrass points from Calflora (CA)	1,720
Random buffer points (200 m radius)	6,880
Total points used in MLP	8,600
Positive samples (probability $>$ 0.4)	2,108
Positive samples (probability $>$ 0.5)	1,629
Positive samples (probability $>$ 0.6)	1,196
Positive samples (probability $>$ 0.7)	712

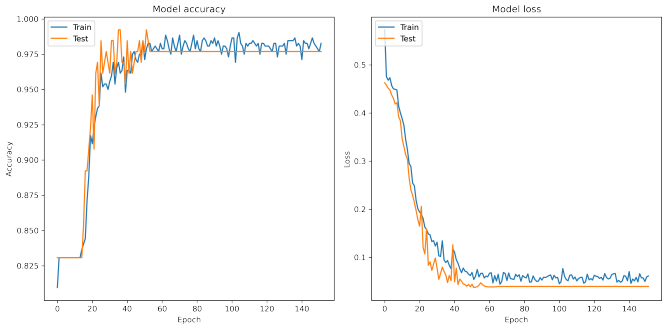

Fig. 15: Loss and Accuracy curve of MLP Classifier.

B. Mojave Desert

The Mojave Desert landscape is primarily characterized by bare land and shrubland[59]; however, instances of Cheatgrass (Bromus tectorum) emergence have also been observed following fire events[60]. Our LULC map effectively captures this dynamic, illustrating our model's robustness in mapping diverse terrain and land cover patterns(Figure 16).

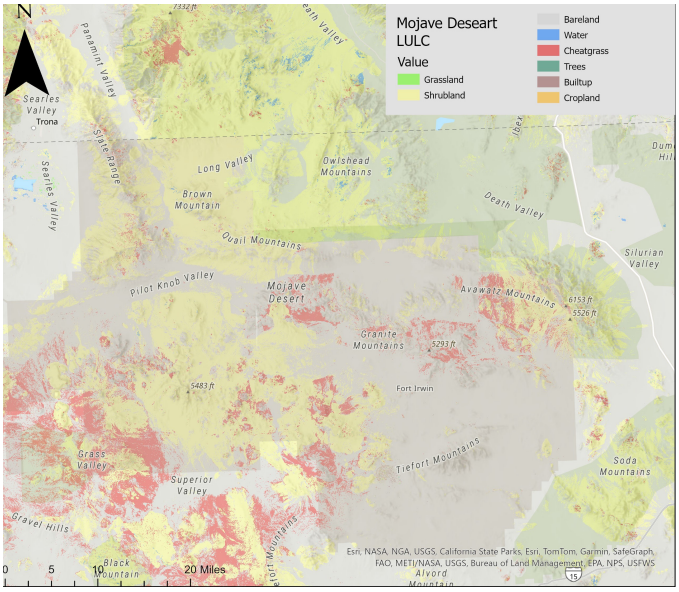

Fig. 16: Mojave Desert 2024 LULC.

REFERENCES

1 Duguy, B., Paula, S., Pausas, J. G., Alloza, J. A., Gimeno, T., and Vallejo, V. R., "Effects of climate and extreme events on wildfire regime and their ecological impacts," in *Advances in Global Change Research*. Berlin, Germany: Springer Science and Business Media LLC, 2012, vol. 51, pp. 101–134, [Google Scholar].

2 Brotons, L., Aquilué, N., De Cáceres, M., Fortin, M.-J., and Fall, A., "How fire history, fire suppression practices and climate change affect wildfire regimes in mediterranean landscapes," *PLoS ONE*, vol. 8, p. e62392, 2013, [Google Scholar] [CrossRef] [Green Version].

3 Wang, Z., Chappellaz, J., Park, K.-R., and Mak, J. E., "Large variations in southern hemisphere biomass burning during the last 650 years," *Science*, vol. 330, pp. 1663–1666, 2010, [Google Scholar] [CrossRef] [Green Version].

4 Safford, H. D., Paulson, A. K., Steel, Z. L., Young, D. J. N., Wayman, R. B., and Varner, M., "The 2020 california fire season: a year like no other, a return to the past or a harbinger of the future?" *Global Ecology and Biogeography*, vol. 31, pp. 2005–2025, 2022.

5 Meng, Y.-Y., Yu, Y., Garcia-Gonzales, D., Al-Hamdan, M. Z., Marlier, M. E., Wilkins, J. L., Ponce, N., and Jerrett, M., "Health and economic cost estimates of short-term total and wildfire pm2.5 exposure on work loss: using the consecutive california health interview survey (chis) data 2015–2018," *BMJ Public Health*, vol. 2, p. e000491, 2024.

6 Commission, C. E., "California's fourth climate change assessment," California Energy Commission, Tech. Rep., 2018. [Online]. Available: https://www.energy.ca.gov/sites/default/files/2019-12/Forests_CCCA4-CNRA-2018-008_ada.pdf

7 Holden, Z. A., Swanson, A., Luce, C. H., Jolly, W. M., Maneta, M., Oyler, J. W., Warren, D. A., Parsons, R., and Affleck, D., "Decreasing fire season precipitation increased recent western us forest wildfire activity," *Proceedings of the National Academy of Sciences*, vol. 115, no. 36, pp. E8349–E8357, 2018. [Online]. Available: https://www.pnas.org/doi/abs/10.1073/pnas.1802316115

8 Abouali, A., Viegas, D. X., and Raposo, J. R., "Analysis of the wind flow and fire spread dynamics over a sloped–ridgeline hill," *Combustion and Flame*, vol. 234, p. 111724, 2021. [Online]. Available: https://www.sciencedirect.com/science/article/pii/S0010218021004673

9 National Interagency Fire Center, "Annual report 2013," 2013, accessed: 2024-05-31. [Online]. Available: https://www.nifc.gov/sites/default/files/NICC/2-Predictive%20Services/Intelligence/Annual%20Reports/2013/Annual_Report_2013_508.pdf

10 Flannigan, M. *et al.*, "Lightning-ignited forest fires in northwestern ontario," *Canadian Journal of Forest Research*, vol. 21, no. 4, pp. 395–402, 1991.

11 Collins, K. M., Penman, T. D., and Price, O. F., "Some wildfire ignition causes pose more risk of destroying houses than others," *PLOS ONE*, vol. 11, no. 9, pp. 1–18, 09 2016. [Online]. Available: https://doi.org/10.1371/journal.pone.0162083

12 Penman, T. D., Bradstock, R. A., and Price, O., "Modelling the determinants of ignition in the sydney basin, australia: implications for future management," *International Journal of Wildland Fire*, vol. 22, pp. 469–478, 2013.

13 Freeman, E. D., Sharp, T. R., Larsen, R. T., Knight, R. N., Slater, S. J., and McMillan, B. R., "Negative effects of an exotic grass invasion on small-mammal communities," *PLoS One*, vol. 9, no. 9, p. e108843, 2014.

14 Holbrook, J. D., Arkle, R. S., Rachlow, J. L., Vierling, K. T., Pilliod, D. S., and Wiest, M. M., "Occupancy and abundance of predator and prey: implications of the fire-cheatgrass cycle in sagebrush ecosystems," *Ecosphere*, vol. 7, no. 6, p. e01307, 2016.

15 Crawford, J. A., Olson, R. A., West, N. E., Mosley, J. C., Schroeder, M. A., Whitson, T. D., Miller, R. F., Gregg, M. A., and Boyd, C. S., "Ecology

and management of sage-grouse and sage-grouse habitat," *Journal of Range Management*, vol. 57, no. 1, pp. 2–19, 2004.
16 Lockyer, Z. B., Coates, P. S., Casazza, M. L., Espinosa, S., and Delehanty, D. J., "Nest-site selection and reproductive success of greater sage-grouse in a fire-affected habitat of northwestern nevada," *The Journal of Wildlife Management*, vol. 79, no. 5, pp. 785–797, 2015.
17 Balch, J. K., Bradley, B. A., D'Antonio, C. M., and Gómez-Dans, J., "Introduced annual grass increases regional fire activity across the arid western usa (1980–2009)," *Global change biology*, vol. 19, no. 1, pp. 173–183, 2013.
18 Pilliod, D. S., Welty, J. L., and Arkle, R. S., "Refining the cheatgrass–fire cycle in the great basin: Precipitation timing and fine fuel composition predict wildfire trends," *Ecology and Evolution*, vol. 7, no. 19, pp. 8126–8151, 2017.
19 Davies, K. W. and Nafus, A. M., "Exotic annual grass invasion alters fuel amounts, continuity and moisture content," *International journal of wildland fire*, vol. 22, no. 3, pp. 353–358, 2012.
20 Wolkovich, E. M. and Cleland, E. E., "The phenology of plant invasions: a community ecology perspective," *Frontiers in Ecology and the Environment*, vol. 9, no. 5, pp. 287–294, 2011.
21 Bradley, B. A., "Remote detection of invasive plants: a review of spectral, textural and phenological approaches," *Biological invasions*, vol. 16, pp. 1411–1425, 2014.
22 Peterson, E., "Estimating cover of an invasive grass (bromus tectorum) using tobit regression and phenology derived from two dates of landsat etm+ data," *International Journal of Remote Sensing*, vol. 26, no. 12, pp. 2491–2507, 2005.
23 Pandey, P. C., Koutsias, N., Petropoulos, G. P., Srivastava, P. K., and Dor, E. B., "Land use/land cover in view of earth observation: data sources, input dimensions and classifiers – a review of the state of the art," *Geocarto International*, pp. 1–38, 2019.
24 Lang, R., Shao, G., Pijanowski, B. C., and Farnsworth, R. L., "Optimizing unsupervised classifications of remotely sensed imagery with a data-assisted labeling approach," *Computers & Geosciences*, vol. 34, no. 12, pp. 1877–1885, 2008.
25 Omo-Irabor, O., "A comparative study of image classification algorithms for landscape assessment of the niger delta region," *Journal of Geographic Information System*, vol. 8, pp. 163–170, 2016.
26 Polat, N. and Kaya, Y., "Investigation of the performance of different pixel-based classification methods in land use/land cover (lulc) determination," *Türkiye İnsansız Hava Araçları Dergisi*, vol. 3, pp. 1–6, 2021.
27 United States Department of Agriculture, "Fuelscape data for wildfire risk assessment in the sagebrush biome of the western united states," 2024, accessed: 2024-05-31. [Online]. Available: https://www.fs.usda.gov/rds/archive/catalog/RDS-2024-0004
28 Pastick, N. J., Dahal, D., Wylie, B. K., Parajuli, S., Boyte, S. P., and Wu, Z., "Characterizing land surface phenology and exotic annual grasses in dryland ecosystems using landsat and sentinel-2 data in harmony," *Remote Sensing*, vol. 12, no. 4, 2020. [Online]. Available: https://www.mdpi.com/2072-4292/12/4/725
29 Department, S. B. C. F., "Santa barbara county fire department official website," 2024, accessed: October 22, 2024. [Online]. Available: https://sbcfire.com/
30 Calflora, "Calflora: Information on california plants for education, research and conservation," https://www.calflora.org/, 2024, accessed: 2024-01-10.
31 European Space Agency (ESA), "Sentinel-2 data," 2024, accessed: 2024-07-05. [Online]. Available: https://dataspace.copernicus.eu/explore-data/data-collections/sentinel-data/sentinel-2
32 Gorelick, N., Hancher, M., Dixon, M., Ilyushchenko, S., Thau, D., and Moore, R., "Google earth engine: Planetary-scale geospatial analysis for everyone," *Remote Sensing of Environment*, vol. 202, pp. 18–27, 2017.
33 Dodgson, N. A., "Quadratic interpolation for image resampling," *IEEE transactions on image processing*, vol. 6, no. 9, pp. 1322–1326, 1997.
34 names as per the article (replace this placeholder), A., "Title of the article (replace this placeholder)," *Remote Sensing*, vol. 13, no. 8, p. 1494, 2021. [Online]. Available: https://www.mdpi.com/2072-4292/13/8/1494
35 Google Earth Engine Developers, "COPERNICUS_S2_SR Bands," Google Earth Engine Dataset Catalog, 2024, accessed: 2024-03-22. [Online]. Available: https://developers.google.com/earth-engine/datasets/catalog/COPERNICUS_S2_SR\#bands
36 Spatial Thoughts, "Extracting time series using google earth engine," Spatial Thoughts, 4 2020, accessed: 2024-03-22. [Online]. Available: https://spatialthoughts.com/2020/04/13/extracting-time-series-ee/
37 Esri, "Arcgis pro," https://www.esri.com/en-us/arcgis/products/arcgis-pro/overview, 2024, accessed: 2024-06-13.
38 Britannica, E., "Los angeles: Landscape," n.d., accessed: 2024-10-09. [Online]. Available: https://www.britannica.com/place/Los-Angeles-California/Landscape
39 Engine, G. E., "Dynamic world v1 land cover," https://developers.google.com/earth-engine/datasets/catalog/GOOGLE_DYNAMICWORLD_V1, 2022, accessed: 2024-06-13.
40 Bureau of Land Management, "The great basin restoration initiative, a hand to nature: progress to date," 2001, available online at: www.fire.blm.gov/gbri/docs/gbri_progress_901.pdf (accessed 24 September 2007).
41 Bishop, C. M., *Pattern Recognition and Machine Learning*. Springer, 2006.
42 iNaturalist, "Observations: Cheatgrass (bromus tectorum)," 2024, accessed: 2024-07-06. [Online]. Available: https://www.inaturalist.org/observations?place_id=any&subview=map&taxon_id=164056
43 Rouse, J., Haas, R., Schell, J., and Deering, D., "Monitoring vegetation systems in the great plains with erts," *Proceedings of the Third Earth Resources Technology Satellite-1 Symposium*, vol. 1, pp. 309–317, 1974.
44 Gitelson, A. and Merzlyak, M., "Signature analysis of leaf reflectance spectra: Algorithm development for remote sensing of chlorophyll," *Journal of Plant Physiology*, vol. 148, no. 3-4, pp. 494–500, 1996.
45 Qi, J., Chehbouni, A., Huete, A., Kerr, Y., and Sorooshian, S., "A modified soil adjusted vegetation index (msavi)," *Remote Sensing of Environment*, vol. 48, no. 2, pp. 119–126, 1994.
46 Chen, T. and Guestrin, C., "Xgboost: A scalable tree boosting system," in *Proceedings of the 22nd acm sigkdd international conference on knowledge discovery and data mining*, 2016, pp. 785–794.
47 Abdi, A. M., "Land cover and land use classification performance of machine learning algorithms in a boreal landscape using sentinel-2 data," *GIScience & Remote Sensing*, vol. 57, no. 1, pp. 1–20, 2020.
48 Shiferaw, H., Bewket, W., and Eckert, S., "Performances of machine learning algorithms for mapping fractional cover of an invasive plant species in a dryland ecosystem," *Ecology and evolution*, vol. 9, no. 5, pp. 2562–2574, 2019.
49 Man, C. D., Nguyen, T. T., Bui, H. Q., Lasko, K., and Nguyen, T. N. T., "Improvement of land-cover classification over frequently cloud-covered areas using landsat 8 time-series composites and an ensemble of supervised classifiers," *International Journal of Remote Sensing*, vol. 39, no. 4, pp. 1243–1255, 2018.
50 Breiman, L., "Random forests," *Machine learning*, vol. 45, pp. 5–32, 2001.
51 Hunter, F., Mitchard, E., Tyrrell, P., and Russell, S., "Inter-seasonal time series imagery enhances classification accuracy of grazing resource and land degradation maps in a savanna ecosystem," *Remote Sens.*, vol. 12, p. 198, 2020, [CrossRef] [Green Version]. [Online]. Available: https://www.mdpi.com/2072-4292/12/1/198
52 Bradter, U., O'Connell, J., Kunin, W., Boffey, C., Ellis, R., and Benton, T., "Classifying grass-dominated habitats from remotely sensed data: The influence of spectral resolution, acquisition time and the vegetation classification system on accuracy and thematic resolution," *Science of The Total Environment*, vol. 711, p. 134584, 2020, [CrossRef]. [Online]. Available: https://linkinghub.elsevier.com/retrieve/pii/S0048969719345759
53 Strobl, C., Malley, J., and Tutz, G., "An introduction to recursive partitioning: rationale, application, and characteristics of classification and regression trees, bagging, and random forests." *Psychological methods*, vol. 14, no. 4, p. 323, 2009.
54 Wikipedia contributors, "El dorado fire," 2024, accessed: 2024-05-31. [Online]. Available: https://en.wikipedia.org/wiki/El_Dorado_Fire
55 Cal Fire, "Corral fire incident updates," https://www.fire.ca.gov/incidents/2024/6/1/corral-fire/updates, 2024, accessed: 2024-06-13.
56 National Interagency Fire Center, "Incident management situation report," June 2024, accessed: 2024-06-14. [Online]. Available: https://www.nifc.gov/sites/default/files/NICC/1-Incident%20Information/IMSR/2024/June/IMSR_CY24_06062024_0.pdf
57 European Commission, Joint Research Centre, "Jrc ghsl p2023a ghs built-up grid," https://developers.google.com/earth-engine/datasets/catalog/JRC_GHSL_P2023A_GHS_BUILT_C, accessed: 2024-07-07.
58 U.S. Department of Agriculture, National Agricultural Statistics Service, "Usda nass cropland data layer," https://developers.google.com/earth-engine/datasets/catalog/USDA_NASS_CDL, accessed: 2024-07-07.
59 Author(s), "Title of the document," Year, retrieved from CiteSeerX. [Online]. Available: https://citeseerx.ist.psu.edu/document?repid=rep1&type=pdf&doi=6eb2aebd61f83cd3aaff8e68878af721913ef911
60 United States Geological Survey (USGS), "Invasive plant cover in the mojave desert, 2009-2013, ver 2.0, april 2021," 2021, accessed: [insert date you accessed this]. [Online]. Available: https://www.usgs.gov/data/invasive-plant-cover-mojave-desert-2009-2013-ver-20-april-2021